

Thermal Transport in Molecular Forests

Aashish Bhardwaj, A. Srikantha Phani, Alireza Nojeh, and Debashish Mukherji*



Cite This: *ACS Nano* 2021, 15, 1826–1832



Read Online

ACCESS |



Metrics & More



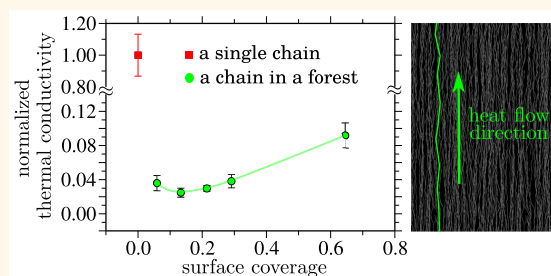
Article Recommendations



Supporting Information

ABSTRACT: Heat propagation in quasi-one-dimensional materials (Q1DMs) often appears puzzling. For example, while an isolated Q1DM, such as a nanowire, a carbon nanotube, or a polymer, can exhibit a high thermal conductivity κ , forests of the same materials can show a reduction in κ . Until now, the complex structures of these assemblies have hindered the emergence of a clear molecular picture for this intriguing phenomenon. We combine coarse-grained simulations with concepts known from polymer physics and thermal transport to unveil a generic microscopic picture of κ reduction in molecular forests. We show that a delicate balance among the persistence length of the Q1DM, the segment orientations, and the flexural vibrations governs the reduction in κ .

KEYWORDS: generic modeling, thermal transport, quasi-one-dimensional materials, persistence length, molecular forests, heat localization



Thermal transport properties are important for heat management in devices, energy generation and storage, electronic packaging, house-hold items, biomaterials, and interfacial composites.^{1–6} For example, a low thermal conductivity κ is desirable for thermoelectrics,^{7–9} while high κ values are needed for heat sinking applications.^{3,10,11} The ability to tune thermal properties is thus broadly important, and nanoscale systems present a great opportunity in this regard because they often exhibit unexpected behavior.¹² Understanding heat transport in quasi-one-dimensional materials (Q1DMs) is a major scientific problem¹² and becomes even more challenging when dealing with arrays of Q1DMs such as forests,^{13–19} bundles,²⁰ sheets,²¹ fibers,^{22,23} and networks.²⁴ In these systems, the complex molecular structures introduce entropic disorder and thus control the physical properties. One such intriguing phenomenon is strong heat localization in carbon nanotube (CNT) forests:¹⁴ while a single CNT may exhibit $\kappa_{\parallel} > 10^3 \text{ Wm}^{-1}\text{K}^{-1}$,^{2,4,5,25} CNT forests show a drastic reduction in κ_{\parallel} . Here, κ_{\parallel} is the thermal conductivity along the molecular backbone. This “heat trap” effect was observed at very high temperatures of $T > 10^3 \text{ K}$. However, room temperature experiments have also yielded relatively low values, such as $\kappa_{\parallel} \approx 0.5\text{--}1.2 \text{ Wm}^{-1}\text{K}^{-1}$ for CNT forests,¹³ $\kappa_{\parallel} \approx 100 \text{ Wm}^{-1}\text{K}^{-1}$ for CNT bundles,²⁰ or $\kappa_{\parallel} \approx 43 \text{ Wm}^{-1}\text{K}^{-1}$ for CNT sheets.²¹ We note that the observed influence of crowding on κ_{\parallel} in CNT forests and sheets may not be a system specific phenomenon. The other examples include nanowire (NW) arrays,^{16–18} polyethylene (PE) fibers,²² crystalline assemblies of PE²³ and poly-3,4-ethylenedioxythiophene (PEDOT),²⁶ and composite materials.²⁷

Heat transport in an isolated Q1DM has been studied extensively.^{12,28–32} Moreover, a few studies have also investigated the effects of crowding on κ , where individual molecules are randomly orientated in a sample.^{33,34} In these studies, the nonbonded van der Waals (vdW) contacts between different Q1DMs strongly influence their thermal behavior, especially when the contour lengths are smaller than the sample dimensions. This vdW-based interaction also leads to a low κ .³³ A molecular forest, however, is inherently anisotropic (*i.e.*, $\kappa_{\parallel} \neq \kappa_{\perp}$), and a delicate balance between the bonded interactions and molecular entanglements is expected to dictate the behavior of κ_{\parallel} along the molecular orientations, while κ_{\perp} is dominated by the weak vdW interaction. Generally, κ between purely bonded neighbors is about 50–100 times larger than that between the nonbonded neighbors.²² Therefore, it is challenging to predict *a priori* how crowding can account for a drop in κ_{\parallel} .^{14,17,18,21,23,26}

In this work, we study the anisotropic heat flow in molecular forests using a multiscale molecular simulation approach. To this end, we (1) devise a generic scheme to map the nanoscale physics onto a coarse-grained (CG) model, (2) develop a microscopic understanding of the reduced heat transport in molecular forests, and (3) imply how a broad range of materials can be modeled within a unified physical framework.

Received: November 20, 2020

Accepted: January 12, 2021

Published: January 15, 2021



To achieve the above goals, we combine molecular dynamics simulations of a generic polymer brush model³⁵ with known theoretical concepts from polymer physics³⁶ and thermal transport.^{37,38}

We consider a Q1DM as a linear polymer chain, where the inherent flexibility is governed by its persistence length l_p . For example, a linear molecule behaves as a rigid rod when the contour length $l_c \simeq l_p$, while it follows self-avoiding random walk statistics for $l_c \gg l_p$.³⁶ In this context, a recent experiment has measured that l_p of an isolated single walled CNT is about 50–60 μm for a CNT diameter of $D \simeq 1.0\text{ nm}$.³⁹ Furthermore, $l_p \simeq 5\mu\text{m}$ for a NW with $D \simeq 1.0\text{ nm}$,⁴⁰ $l_p \simeq 0.65\text{ nm}$ for PE⁴¹, and $l_p \simeq 1.0\text{ nm}$ for PEDOT.⁴² Using these l_p estimates, we can analyze different molecular forests.

For example, the typical heights \mathcal{H} of CNT forests or arrays of NWs range from 0.1 to 2 mm,^{14,43} while in some cases they can reach several millimeters¹³ to even a few centimeters.⁴⁴ For bundles of PE²² or PEDOT,²⁶ $\mathcal{H} \simeq 100\text{ nm}$. Therefore, it is evident that $\mathcal{H} \simeq 2 - 200l_p$ in most cases. This insight provides an important length scale in our simulations and suggests that a long Q1DM can be modeled as a flexible polymer chain and, hence, a molecular forest, as a polymer brush. Here, it is important to note that the bonded monomers along an isolated chain backbone impart almost a crystalline structure, while a polymer brush is amorphous-like in all directions. This is very similar to the situation in molecular forests.^{14,17,18,21,23,26} It should be emphasized that, while a simple polymer model is certainly not appropriate to describe all the complex properties of Q1DMs, our aim is to investigate if a CG model can explain the anomalies in thermal behavior observed in the experiments.^{14,20,21} Furthermore, CNTs and NWs have rather large l_p values of $\simeq 5-50\mu\text{m}$ even when their $D \approx 1.0\text{ nm}$. Here, we map one l_p onto a monomer bead. This simple mapping scheme is chosen to capture the molecular bending for $l_c \geq l_p$, which is essential in dictating the phonon mean-free path and thus κ_{\parallel} in the molecular forests. The details of the simulation model are shown in the [Methods](#) section and the [Supporting Information](#).

RESULTS AND DISCUSSION

Surface Coverage Dependent Thermal Conductivity.

In [Figure 1](#), we summarize the normalized thermal conductivity along a chain backbone $\bar{\kappa}_{\parallel} = \kappa_{\parallel}(\Gamma)/\kappa_{\parallel}(0)$ as a function of surface coverages Γ . Here, $\kappa_{\parallel}(0)$ corresponds to the single chain data (*i.e.*, $\Gamma \rightarrow 0$). Note that for the calculation of κ_{\parallel} in a brush, we only consider one chain in the crowded environment. It can be seen that, within the range of $0.05 < \Gamma < 0.30$, κ_{\parallel} decreases by a factor of 25–30 in a brush compared to a single chain. This sharp decrease is reminiscent of the reduced κ_{\parallel} in CNT forests^{14,20} and sheets.²¹ What causes such a dramatic decrease in κ_{\parallel} ? It is particularly puzzling given that $\Gamma \gg \Gamma^*$ in all cases, where Γ^* is the critical surface coverage, and therefore, individual chains in a brush are expected to stretch significantly;³⁶ see [Table S1](#). Here, κ_{\parallel} is expected to be dominated by the bonded interactions. In this context, a closer investigation reveals that a monomer of a chain in a crowded environment has two different modes of heat dissipation: (a) two covalently bonded neighbors and (b) n nonbonded neighbors governed by the vdW interactions. Furthermore, the vdW interaction strength is less than $k_B T$, while the bonded

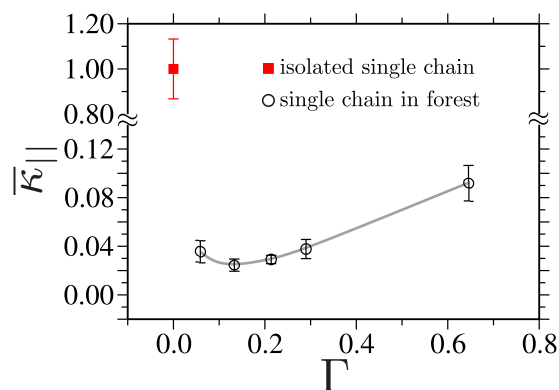


Figure 1. Normalized thermal conductivity along a chain backbone $\bar{\kappa}_{\parallel} = \kappa_{\parallel}(\Gamma)/\kappa_{\parallel}(0)$ as a function of surface coverage of polymers Γ . $\kappa_{\parallel}(0)$ corresponds to the single chain data (*i.e.*, $\Gamma \rightarrow 0$), where the chain is tethered at both ends. For the simulations under crowded environments, we have only calculated κ_{\parallel} of a single chain in a brush configuration, such that a chain experiences a cylinder-like confinement. Note that normalization volume in the Kubo-Green formula is taken as the volume of one chain, *i.e.*, $v = v_m N_l$ with v_m being the volume of one monomer. The gray line is a polynomial fit to the data and is drawn to guide the eye.

interactions can be typically of the order of $80k_B T$ (a number representative of a C–C covalent bond).⁴⁵ The stronger bonded interaction also leads to about 2 orders of magnitude higher stiffness.^{46,47} Moreover, given that κ is directly related to the stiffness (we will come back to this point later),^{37,38} we will now investigate how a 25–30 times reduction in κ_{\parallel} is observed in [Figure 1](#) and in the experiments.^{13,14,20,21} For this purpose, we will investigate the influence of microscopic chain structure and orientation on κ_{\parallel} .

Bond Orientation, Stress, and Thermal Conductivity.

We start by calculating the second Legendre polynomial P_2 of the bond orientation vector using $P_2 = (3\langle \cos^2(\theta) \rangle - 1)/2$. Here, θ is the angle of a bond vector with the z axis and $\langle \cdot \rangle$ represents the average over all bonds and the simulation time. When $P_2 = 1.0$, all bonds are oriented along the z axis (*i.e.*, the direction of chain orientation in a forest); $P_2 = 0.0$ when bonds are randomly oriented, and $P_2 = -1/2$ when all bonds are perpendicular to the z axis. In [Figure 2a](#), we show the variation of P_2 with the elevation h of the brushes for four different Γ values. It can be seen that $P_2 \simeq 0.92$ for a single polymer with about 5% fluctuation. This is expected given that a single chain is fully extended and all bonded monomers are arranged in an almost perfect one-dimensional crystalline structure along the z axis. This is also consistent with a large κ_{\parallel} value for a single chain (see [Figure 1](#)).

For $\Gamma = 0.13$ in [Figure 2a](#), it can be seen that P_2 decreases sharply with h , as expected from the structure of the polymer brushes.^{48–50} This is consistent with the tethering constraint that the chains are significantly more stretched near the tethered points and become more randomly oriented as h increases; see also simulation snapshots in [Figure 2b](#). Furthermore, the individual chain end-to-end distances are $R_{ee}^z \simeq 370d$ (see [Table S1](#) and [Figure S1](#)), which is only about 75% of the chain contour length $l_c = N_l l_b \simeq 485d$ (*i.e.*, for $N_l = 500$). Here, d is the unit of length in the generic model (see the [Methods](#) section). This difference between R_{ee}^z and l_c indicates a significant chain bending and introduces kinks along the chain contour, as shown in the lower panels of the

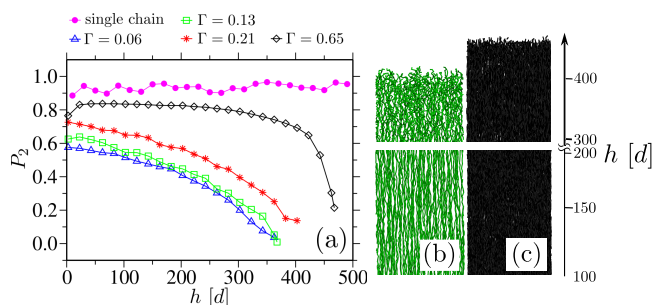


Figure 2. Panel (a) shows the second Legendre polynomial of the bond orientation vector P_2 as a function of the brush elevation height h along the z axis (*i.e.*, the direction of chain orientation in a forest). Data are shown for a single chain and for four different surface coverages Γ . For clarity of presentation, only two simulation snapshots are shown, *i.e.*, corresponding to the minimum and maximum values of $\bar{\kappa}_{\parallel}$ (see Figure 1) for $\Gamma = 0.13$ and $\Gamma = 0.65$ in parts (b) and (c), respectively. The systems are equilibrated using the protocol described in the Methods section at the end of this text. The bottom panels of the snapshots are the enlarged views of brushes between $100d < h < 200d$, and the top panels show the top layer for $h > 340d$ with d being the unit of length in the generic model. The arrow at the right corner points at the direction of h . The lines are drawn to guide the eye.

simulation snapshots in Figure 2b. With increasing h , chain bending (or kinks) become increasingly prominent, see the upper panels of the simulation snapshots in Figure 2b. In this context, it is important to note that, in a fully extended chain (as in our case of the single chain), phonon-like wave propagation carries a heat current along the chain backbone because of the periodic arrangement of monomers. When kinks appear along a chain backbone due to the flexural vibrations dictated by l_p (as in the cases of $\Gamma = 0.13$), the longitudinal phonon propagation is impacted. Here, each kink acts as a scattering center for phonon propagation and thus reduces the phonon mean free path. The larger the number of kinks for a given N_l , the higher is the resistance to heat flow, *i.e.*, the lower the κ_{\parallel} (see Figure 1). This observation is consistent with the recent simulation study of a single PE chain, where it has been shown that increasing the number of kinks also decreases κ_{\parallel} .⁵¹ The same also holds for $\Gamma = 0.06$ and 0.21 . For $\Gamma = 0.65$, bonds are significantly more oriented along the direction of the brush growth and also the chains are more stretched with $R_{ee}^z \simeq 450d$ (see Figure 2a,c), resulting in an approximately 3-fold increase of κ_{\parallel} in comparison to $0.05 \leq \Gamma \leq 0.30$; see Figure 1. We also note that, while κ_{\parallel} decreases by over 90% between the single chain and $\Gamma = 0.65$, P_2 changes only about 5–10% between the two cases. This can be understood on the basis of two observations: (1) Even when the individual chains in a forest with $\Gamma = 0.65$ are significantly extended (*i.e.*, following a step like density profile, see Figure S1), they still have many kinks along the chain contour; it has been shown that even a small number of kinks can significantly reduce κ_{\parallel} .⁵¹ (2) An increase in Γ also increases monomer–monomer nonbonded contacts and provides an additional pathway for heat leakage. This significantly increases κ_{\perp} in the lateral directions, *i.e.*, the x and y directions. See Figure S3b, where it is evident that κ_{\perp} increases by an order of magnitude between $\Gamma = 0.13$ and $\Gamma = 0.65$.

The delicate balance of the heat leakage between two bonded and n nonbonded monomers may also explain the

subtle increase in κ_{\parallel} for $\Gamma = 0.06$ in comparison to $\Gamma = 0.13$; see Figure 1. More specifically, while P_2 only decreases by about 5% for $\Gamma = 0.06$ in comparison to $\Gamma = 0.13$ (see Figure 2a), the monomer density ρ decreases by almost 50% (see Figure S1). This decrease in ρ also reduces the rate of heat leakage between the nonbonded neighbors, as seen by about a 7-fold decrease in κ_{\perp} (see Figure S3b), and thus plays an important role in dictating the behavior of κ_{\parallel} . Moreover, the exact relationship between κ_{\parallel} and κ_{\perp} is rather nontrivial that we will discuss at a later stage of this work.

Chain bending also reduces the longitudinal chain stiffness and thus κ . Therefore, to achieve a better quantitative relationship between P_2 (or an estimate of bending), local stiffness, and κ , we will now investigate how P_2 can be related to stiffness (or stress). For this purpose, we have calculated the h dependent bonded contribution to the virial stress σ_{\parallel}^B . The data are shown in Figure 3. It can be seen that the data for $\Gamma =$

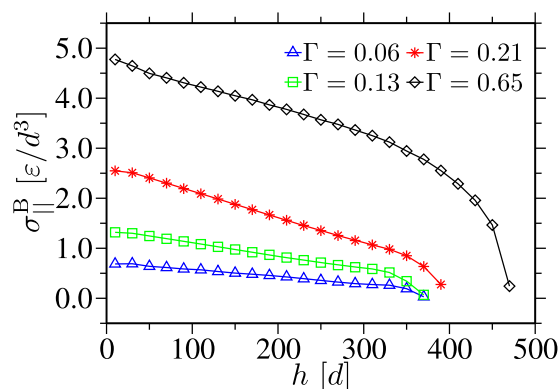


Figure 3. Stress along the chain backbone σ_{\parallel}^B as a function of the brush elevation height h along the z axis (*i.e.*, the direction of chain orientation in a forest). Data is shown for four different surface coverages Γ . The lines are drawn to guide the eye.

0.06, 0.13, and 0.21 show a large variation with h , but this is significantly lower than $\sigma_{\parallel}^B \simeq 5.0\epsilon/d^3$ for $\Gamma = 0.65$; see the black data set in Figure 3. We highlight that the monomer arrangements in our model system of forests are amorphous in all directions (as evident from Figures 2 and S1), while it is periodic along the contour of an isolated single stretched chain. The amorphous-like structures originate due to the molecular kinks along the z direction (*i.e.*, the direction of chain orientation). This is reflected in the variation of κ_{\parallel} with temperature T (see Figure S4), which does not show the typical T^{-1} scaling expected for heat transport of the standard heat transport in the crystals.^{1,52} Instead, we observe an increase of κ_{\parallel} with T , as known for amorphous materials³ where heat propagates because of the local fluctuations. Furthermore, while phonons carry a heat current in crystalline materials,^{1,52} such a compact phonon picture is absent in amorphous materials^{53,54} as in the case of molecular forests. In this context, a forest with a typical height much larger than the l_p of a Q1DM, such as CNT or NW, will also exhibit kinks and thus include amorphous-like arrangements.

Height Dependent Anisotropic Thermal Conductivity. Figures 2a and 3 also suggest that there is an inherent h dependent anisotropy in the chain orientation; *i.e.*, the chains are more extended very close to $h \rightarrow 0$ due to the tethering constraint and crowding because of increasing Γ . In contrast,

chain orientations become more random with increasing h .^{36,48,49} Consequent anisotropy is reflected in $\kappa_{\parallel}/\kappa_{\perp}$; see Figure 4. For $\Gamma = 0.06$, the heat flow remains highly anisotropic

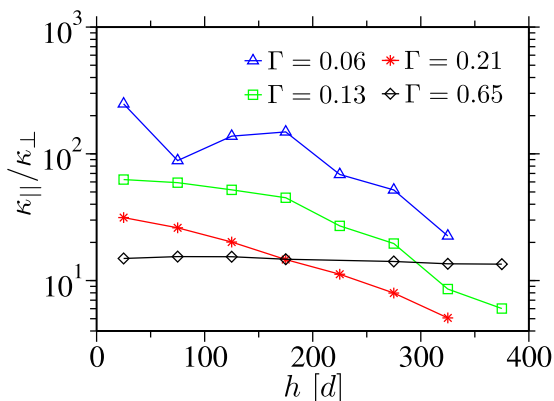


Figure 4. $\kappa_{\parallel}/\kappa_{\perp}$ as a function of the brush elevation height h . Here, κ_{\parallel} and κ_{\perp} are the parallel and the perpendicular components of the thermal conductivity, respectively. Data are shown for four different surface coverages Γ . The lines are drawn to guide the eye.

over the full range of $h \rightarrow 300d$, which is because of the drastically reduced κ_{\perp} values (see Figure S3). We also note that a dip in Figure 4 around $h = 75d$ is because of the error associated with the κ_{\perp} calculation; see Figure S3b and Section S2 for details. Moreover, for $\Gamma = 0.13$, we observe that heat flow is highly anisotropic for $h < 200d$ ($\kappa_{\parallel}/\kappa_{\perp} \approx 50\text{--}60$), moderately anisotropic for $200d < h < 350d$ ($\kappa_{\parallel}/\kappa_{\perp} \approx 10\text{--}40$), and weakly anisotropic for $h > 350d$ ($\kappa_{\parallel}/\kappa_{\perp} < 10$). With increasing Γ , the relative anisotropy in $\kappa_{\parallel}/\kappa_{\perp}$ decreases (see the green and red data sets in Figure 4). This is predominantly because of the increased particle number density ρ that induces a faster increase in κ_{\perp} than κ_{\parallel} with ρ (see Figures S1 and S3 and Section S2). Considering that $l_p \approx 1d$ in our model, this also gives a comparable estimate of the relevant length scales (in terms of l_p) that are needed to make a direct experimental comparison. In this context, most experiments on CNT forests dealing with $\Gamma \leq 0.10$ involve \mathcal{D} values of a few nanometers to a few tens of nanometers and also relatively small \mathcal{H} values of ≤ 2 mm.¹⁴ Therefore, these conditions typically fall within the range where \mathcal{H} varies from a few l_p to about $40l_p$ (*i.e.*, for $\mathcal{D} \approx 1.0$ nm and $\mathcal{H} \approx 2$ mm).³⁹ This will then lead to a rather anisotropic regime.^{14,21} Experiments on CNT forests yielded a $\kappa_{\parallel}/\kappa_{\perp}$ of $\approx 10\text{--}100$,¹³ for CNT sheets, $\kappa_{\parallel}/\kappa_{\perp} \approx 500$,²¹ and for PE fibers, $\kappa_{\parallel}/\kappa_{\perp} \approx 1000$.²² Our simulations show $\kappa_{\parallel}/\kappa_{\perp} \approx 10\text{--}60$ for $h < 200l_p$ and with varying Γ ; see Figure 4. This further suggests that our simple CG model captures the relevant physics of the problem.

Lastly, we investigate the dependence of κ_{\parallel} on the material's stiffness.³⁷ Figure 5 shows κ_{\parallel} as a function of an estimate of the elastic modulus E along the direction of the chain orientation. Given that the bond stretching remains small, we use $E = \sigma_{\parallel}^B/\mathcal{E}$. Here, \mathcal{E} is strain. We estimate \mathcal{E} from the stretching of the bond vector along the z direction, which is only about 1.0% for $\Gamma = 0.13$, 1.1% for $\Gamma = 0.21$, and 3.0% for $\Gamma = 0.65$. These small \mathcal{E} values are expected for the finitely extensible nonlinear elastic (FENE) bond,³⁵ which can have up to 3.4% fluctuation at $T = 1\epsilon/k_B$. It can be observed that, for $\Gamma = 0.13$ and 0.21 in Figure 5, $\kappa \propto E$, as predicted earlier.^{37,38} For

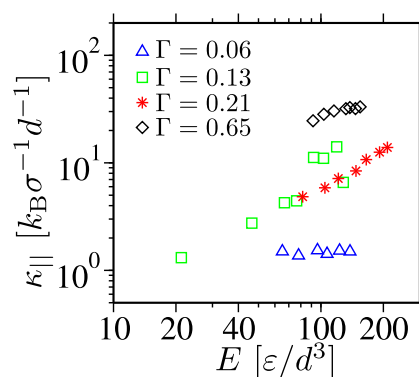


Figure 5. Component of the thermal conductivity along the chain orientation direction κ_{\parallel} as a function of an estimated elastic modulus along the chain orientation $E = \sigma_{\parallel}^B/\mathcal{E}$. Here, σ_{\parallel}^B and \mathcal{E} are the longitudinal bonded components of the stress and the strain estimate, respectively. Data are shown for four different surface coverages Γ .

$\Gamma = 0.06$ and 0.65 , no explicit functional dependence is observed, which is predominantly because of the flat κ_{\parallel} data sets in Figure S3a.

CONCLUSIONS

Combining molecular dynamics simulations with known concepts from polymer physics and thermal conductivity, we have studied the microscopic, generic behavior of anisotropic thermal conductivity in molecular forests. As a model system, we have used a generic coarse-grained polymer brush. We provide a possible explanation for the reduced thermal conductivity in molecular forests, *i.e.*, the observation that, while a single linear molecule can have very large thermal conductivity along the molecular backbone κ_{\parallel} , the same molecule in a forest shows a drastic reduction in κ_{\parallel} . Typical experimental systems include nanotube and nanowire forests and macromolecular fibers. Our analysis reveals that the reduced κ_{\parallel} is due to the delicate balance between the lateral chain bending that hinders the longitudinal heat flow along the molecular backbone and the lateral heat leakage between the nonbonded neighbors. These results point to a general principle of flexible tuning of κ by changing density, molecular flexibility, and forest height. Therefore, they may be useful for the design of advanced functional materials with tunable thermal properties.

METHODS

Generic Model. For the simulations of polymer brush, we have used the bead–spring model.³⁵ In this model, individual monomers interact with each other *via* a repulsive 6–12 Lennard-Jones potential with a cutoff distance $r_c = 2^{1/6}d$. $V_{LJ} = 0$ for $r > r_c$. The bonded monomers in a chain interact with an additional finitely extensible nonlinear elastic (FENE) potential. The results are presented in the unit of LJ energy ϵ , LJ distance d , and mass m of individual monomers. This leads to a time unit of $\tau = d(m/\epsilon)^{1/2}$. Values that would be representative for hydrocarbons are as follows: $\epsilon = 30$ meV, $d = 0.5$ nm, and $\tau = 3$ ps. The unit of pressure $P_0 = 40$ MPa.³⁵ Simulations are performed using the LAMMPS package,⁵⁵ and the simulation snapshots are rendered using the VMD package.⁵⁶

We consider chains of length $N_j = 500$. Note that l_p of the fully flexible polymer model is about one bead; thus, in our case $N_j \approx 500l_p$. Here, the bond length $l_b \approx 0.97d$. Furthermore, the first monomer of every chain is tethered randomly onto a square plane with lateral dimensions $L_x = L_y \approx 36.5d$, and the chains are oriented

normal to the surface in the z direction. The surface coverage Γ is varied up to 0.65. Γ is calculated as the ratio of the total area occupied by all tethered monomers and the surface area of the plane. The area projection occupied by one monomer onto a surface is estimated by $\pi d^2/4$. Γ values chosen here are much larger than the critical surface coverage defined as $\Gamma^* = (d/2R_g)^2$ with R_g being the bulk radius of gyration of a good solvent chain.^{36,48–50} For a given N_l (or R_g), one chain occupies a surface area πR_g^2 . Periodic boundary conditions are applied in the x and y directions. One set of single chain simulations have also been performed where the chain is tethered at both ends forming a fully stretched configuration.

Simulations are carried out in two stages: the initial equilibration and the thermal transport calculations. The initial equilibration is performed under the canonical ensemble with a time step of $\Delta t = 10^{-2}\tau$. The equations of motion are integrated using the velocity Verlet algorithm.⁵⁷ The system is thermalized *via* a Langevin thermostat with a damping constant $\gamma = 1\tau^{-1}$ and $T = 1\epsilon/k_B$, where k_B is the Boltzmann constant.

It is important to note that our protocol to generate an equilibrated brush configuration reasonably mimics the experimental reality of synthesizing a CNT forest.^{13,14} In experiments, a CNT forest is gradually grown upward starting from the catalyst nanoparticles on a substrate using the process of chemical vapor deposition. In our model system of forests, the chains are grown normal to the substrate with $\Gamma \gg \Gamma^*$; see Table S1. Here, we are dealing with high density brush systems of very long chains; thus, the system equilibration is a nontrivial issue.⁴⁹ Therefore, we have performed a two stage equilibration of these brush systems. In the first step, the excluded volume interaction between the nonbonded monomers is increased from $0d$ to $1d$ with a step of $0.01d$ during a warm up stage for each system. Every time the diameter of a monomer grows by $0.01d$, the system is equilibrated for $10^4\tau$. This equilibration step ensures that the bonds of the different neighboring chains can cross each other, while generating the samples without any unphysical particle–particle overlap, and equilibrates a sample. After this initial warm up stage, another equilibration is performed for $10^6\tau$. These configurations are used for the calculations of the observables, such as κ , σ_{\parallel}^B , P_2 , and ρ . Note that, during the subsequent simulation runs using the above-described equilibrated samples, monomer density ρ (see Figure S1) and virial stress σ_{\parallel}^B profiles (see Figure 3) only change by less than 2%. This further suggests that the simulation configurations have reached a well equilibrated state. The striking similarity between the experimental system and the model system of forests presented here is highlighted by the presence of kinks along the molecular backbone that effects heat propagation along the chain. Further simulation details are shown in Section S1 and Figure S1.

Calculation of Thermal Transport Coefficient Using the Kubo-Green Method. After the initial system preparation and equilibration, the components of κ are calculated using the Kubo-Green method in the microcanonical ensemble⁵⁸ implementation in LAMMPS.⁵⁵ The equations of motion are integrated in the microcanonical ensemble with a time step of $\Delta t = 10^{-3}\tau$, while an estimate of the heat flux autocorrelation function, $C(t) = \langle \mathbf{J}(t) \cdot \mathbf{J}(0) \rangle$, is obtained by sampling the heat flux vector $\mathbf{J}(t)$. Here, the correlation function is sampled over a time frame of $0 \leq t \leq 2 \times 10^3\tau$, which is 1 order of magnitude larger than the typical decorrelation time. During a total simulation of $2 \times 10^5\tau$, we accumulate correlation data and compute a running average of the heat flux correlation function $C(t)$. In Figure S2, we show the typical $C(t)$ data for a few of our simulation runs. Finally, κ values are calculated by taking the plateau value of the Green–Kubo integral for the component along the chain orientation direction,

$$\kappa_{\parallel} = \frac{v}{k_B T^2} \int_0^{\infty} \langle \mathbf{J}_z(t) \cdot \mathbf{J}_z(0) \rangle dt \quad (1)$$

and in the lateral directions, *i.e.*, x and y directions,

$$\kappa_{\perp}(t) = \frac{v}{2k_B T^2} \int_0^{\infty} [\langle \mathbf{J}_x(t) \cdot \mathbf{J}_x(0) \rangle + \langle \mathbf{J}_y(t) \cdot \mathbf{J}_y(0) \rangle] dt \quad (2)$$

Note that the volume v of a single chain is used for $\bar{\kappa}_{\parallel}$ calculations in Figure 1 for the consistent comparison with varying Γ . However, for the slab-wise κ_{\parallel} calculations (see Figure S3a), we have used v of the individual slabs, *i.e.*, an absolute κ_{\parallel} estimate.

Stress Calculations. The virial stress σ_{\parallel}^B is calculated using the standard subroutine in LAMMPS⁵⁵ and following the procedure used earlier.⁵⁰ The brush elevation height h dependent stress profile is calculated by dividing the brush height \mathcal{H} into different slabs of width $50d$; see Figure 2e.

ASSOCIATED CONTENT

Supporting Information

The Supporting Information is available free of charge at <https://pubs.acs.org/doi/10.1021/acsnano.0c09741>.

System details, monomer density profiles, and their related explanations, the heat flux autocorrelation functions used for the calculation of κ , height dependent κ_{\parallel} and κ_{\perp} for the different molecular forests, and the temperature effect on κ_{\parallel} and κ_{\perp} (PDF)

AUTHOR INFORMATION

Corresponding Author

Debashish Mukherji – Quantum Matter Institute, University of British Columbia, Vancouver, British Columbia V6T 1Z4, Canada; orcid.org/0000-0002-6242-1754; Email: debashish.mukherji@ubc.ca

Authors

Aashish Bhardwaj – Department of Mechanical Engineering, University of British Columbia, Vancouver, British Columbia V6T 1Z4, Canada

A. Srikantha Phani – Department of Mechanical Engineering, University of British Columbia, Vancouver, British Columbia V6T 1Z4, Canada

Alireza Nojeh – Department of Electrical and Computer Engineering and Quantum Matter Institute, University of British Columbia, Vancouver, British Columbia V6T 1Z4, Canada; orcid.org/0000-0001-8683-1195

Complete contact information is available at: <https://pubs.acs.org/doi/10.1021/acsnano.0c09741>

Notes

The authors declare no competing financial interest. A preliminary version of this work is available at the Physics preprint server.⁵⁹

ACKNOWLEDGMENTS

D.M. thanks Carlos Marques for suggesting refs S3–S5 in the Supporting Information and also for the very insightful discussions on the chain end segregation at the interfaces of the nearly incompressible polymer systems. We thank George Sawatzky, Daniel Bruns, and Manjesh Singh for useful discussions. We further thank Celine Ruscher for a critical reading of the manuscript. This research was undertaken thanks in part to funding from the Canada First Research Excellence Fund (CFREF), Quantum Materials and Future Technologies Program. A.S.P. thanks the NSERC Discovery Grant program for support. A.N. thanks the Natural Sciences and Engineering Research Council of Canada (Grants No. SPG-P 478867, jointly with A.S.P., and No. RGPIN-2017-

04608). D.M. thanks CFREF for financial support. Simulations were performed at the ARC Sockeye facility of the University of British Columbia and the Compute Canada facility, which we take this opportunity to gratefully acknowledge.

REFERENCES

- (1) Cahill, D. G.; Ford, W. K.; Goodson, K. E.; Mahan, G. D.; Majumdar, A.; Maris, H. J.; Merlin, R.; Phillpot, S. R. Nanoscale Thermal Transport. *J. Appl. Phys.* **2003**, *93*, 793–818.
- (2) Berber, S.; Kwon, Y.-K.; Tomanek, D. Unusually High Thermal Conductivity of Carbon Nanotubes. *Phys. Rev. Lett.* **2000**, *84*, 4613–4616.
- (3) Kim, G.; Lee, D.; Shanker, A.; Shao, L.; Kwon, M. S.; Gidley, D.; Kim, J.; Pipe, K. P. High Thermal Conductivity in Amorphous Polymer Blends by Engineered Interchain Interactions. *Nat. Mater.* **2015**, *14*, 295–300.
- (4) Lee, V.; Wu, C.-H.; Lou, Z.-X.; Lee, W.-L.; Chang, C.-W. Divergent and Ultrahigh Thermal Conductivity in Millimeter-Long Nanotubes. *Phys. Rev. Lett.* **2017**, *118*, 135901–5.
- (5) Li, Q.-Y.; Takahashi, K.; Zhang, X. Comment On “Divergent and Ultrahigh Thermal Conductivity in Millimeter-Long Nanotubes. *Phys. Rev. Lett.* **2017**, *119*, 179601–2.
- (6) Fugallo, G.; Colombo, L. Calculating Lattice Thermal Conductivity: A Synopsis. *Phys. Scr.* **2018**, *93*, 043002–23.
- (7) Teweldebrhan, D.; Goyal, V.; Balandin, A. A. Exfoliation and Characterization of Bismuth Telluride Atomic Quintuples and Quasi-Two-Dimensional Crystals. *Nano Lett.* **2010**, *10*, 1209–1218.
- (8) Kodama, T.; Ohnishi, M.; Park, W.; Shiga, T.; Park, J.; Shimada, T.; Shinohara, H.; Shiomi, J.; Goodson, K. E. Modulation of Thermal and Thermoelectric Transport in Individual Carbon Nanotubes by Fullerene Encapsulation. *Nat. Mater.* **2017**, *16*, 892–897.
- (9) Shi, W.; Shuai, Z.; Wang, D. Tuning Thermal Transport in Chain-Oriented Conducting Polymers for Enhanced Thermoelectric Efficiency: A Computational Study. *Adv. Funct. Mater.* **2017**, *27*, 1702847–8.
- (10) Ren, S.; Bernardi, M.; Lunt, R. R.; Bulovic, V.; Grossman, J. C.; Gradecak, S. Toward Efficient Carbon Nanotube/P3HT Solar Cells: Active Layer Morphology, Electrical, and Optical Properties. *Nano Lett.* **2011**, *11*, 5316–5321.
- (11) Smith, M. K.; Singh, V.; Kalaitzidou, K.; Cola, B. A. High Thermal and Electrical Conductivity of Template Fabricated P3HT/MWCNT Composite Nanofibers. *ACS Appl. Mater. Interfaces* **2016**, *8*, 14788–14794.
- (12) Charlier, J. C.; Blase, X.; Roche, S. Electronic and Transport Properties of Nanotubes. *Rev. Mod. Phys.* **2007**, *79*, 677–732.
- (13) Jakubinek, M. B.; White, M. A.; Li, G.; Jayasinghe, C.; Cho, W.; Schulz, M. J.; Shanov, V. Thermal and Electrical Conductivity of Tall, Vertically Aligned Carbon Nanotube Arrays. *Carbon* **2010**, *48*, 3947–3952.
- (14) Yaghoobi, P.; Moghaddam, M. V.; Nojeh, A. Heat Trap”: Light-Induced Localized Heating and Thermionic Electron Emission from Carbon Nanotube Arrays. *Solid State Commun.* **2011**, *151*, 1105–1108.
- (15) Ganguli, S.; Roy, A. K.; Wheeler, R.; Varshney, V.; Du, F.; Dai, L. Superior Thermal Interface via Vertically Aligned Carbon Nanotubes Grown on Graphite Foils. *J. Mater. Res.* **2013**, *28*, 933–939.
- (16) Feser, J. P.; Sadhu, J. S.; Azeredo, B. P.; Hsu, K. H.; Ma, J.; Kim, J.; Seong, M.; Fang, N. X.; Li, X.; Ferreira, P. M.; Sinha, S.; Cahill, D. G. Thermal Conductivity of Silicon Nanowire Arrays with Controlled Roughness. *J. Appl. Phys.* **2012**, *112*, 114306–7.
- (17) Pan, Y.; Hong, G.; Raja, S. N.; Zimmermann, S.; Tiwari, M. K.; Poulidakos, D. Significant Thermal Conductivity Reduction of Silicon Nanowire Forests through Discrete Surface Doping of Germanium. *Appl. Phys. Lett.* **2015**, *106*, 093102–5.
- (18) Pennelli, G.; Elyamny, S.; Dimaggio, E. Thermal Conductivity of Silicon Nanowire Forests. *Nanotechnology* **2018**, *29*, 505402–8.
- (19) Fleming, E.; Du, F.; Ou, E.; Dai, L.; Shi, L. Thermal Conductivity of Carbon Nanotubes Grown by Catalyst-Free Chemical Vapor Deposition in Nanopores. *Carbon* **2019**, *145*, 195–200.
- (20) Jakubinek, M. B. *Nanotube Superfiber Materials, Chapter 16: Thermal Conductivity of Nanotube Assemblies and Superfiber Materials*; Elsevier Publishing Company: Amsterdam, 2014; p 425–456.
- (21) Yamaguchi, S.; Tsunekawa, I.; Komatsu, N.; Gao, W.; Shiga, T.; Kodama, T.; Kono, J.; Shiomi, J. One-Directional Thermal Transport in Densely Aligned Single-Wall Carbon Nanotube Films. *Appl. Phys. Lett.* **2019**, *115*, 223104–5.
- (22) Shen, S.; Henry, A.; Tong, J.; Zheng, R.; Chen, G. Polyethylene Nanofibres with Very High Thermal Conductivities. *Nat. Nanotechnol.* **2010**, *5*, 251–255.
- (23) Henry, A.; Chen, G.; Plimpton, S. J.; Thompson, A. 1D-To-3D Transition of Phonon Heat Conduction in Polyethylene Using Molecular Dynamics Simulations. *Phys. Rev. B: Condens. Matter Mater. Phys.* **2010**, *82*, 144308–5.
- (24) Lian, F.; Llinas, J. P.; Li, Z.; Estrada, D.; Pop, E. Thermal Conductivity of Chirality-Sorted Carbon Nanotube Networks. *Appl. Phys. Lett.* **2016**, *108*, 103101–5.
- (25) Pop, E.; Mann, D.; Wang, Q.; Goodson, K.; Dai, H. Thermal Conductance of an Individual Single-Wall Carbon Nanotube above Room Temperature. *Nano Lett.* **2006**, *6*, 96–100.
- (26) Crnjar, A.; Melis, C.; Colombo, L. Assessing the Anomalous Superdiffusive Heat Transport in a Single One-Dimensional PEDOT Chain. *Phys. Rev. Mater.* **2018**, *2*, 015603–6.
- (27) Hashin, Z. Analysis of Composite Materials- A Survey. *J. Appl. Mech.* **1983**, *50*, 481–505.
- (28) Donadio, D.; Galli, G. Thermal Conductivity of Isolated and Interacting Carbon Nanotubes: Comparing Results from Molecular Dynamics and the Boltzmann Transport Equation. *Phys. Rev. Lett.* **2007**, *99*, 255502–4.
- (29) Henry, A.; Chen, G. High Thermal Conductivity of Single Polyethylene Chains Using Molecular Dynamics Simulations. *Phys. Rev. Lett.* **2008**, *101*, 235502–4.
- (30) Ou, M. N.; Yang, T. J.; Harutyunyan, S. R.; Chen, Y. Y.; Chen, C. D.; Lai, S. J. Electrical and Thermal Transport in Single Nickel Nanowire. *Appl. Phys. Lett.* **2008**, *92*, 063101–3.
- (31) Donadio, D.; Galli, G. Atomistic Simulations of Heat Transport in Silicon Nanowires. *Phys. Rev. Lett.* **2009**, *102*, 195901–4.
- (32) Lee, J.; Lee, W.; Lim, J.; Yu, Y.; Kong, Q.; Urban, J. J.; Yang, P. Thermal Transport in Silicon Nanowires at High Temperature up to 700 K. *Nano Lett.* **2016**, *16*, 4133–4140.
- (33) Prasher, R. S.; Hu, X. J.; Chalopin, Y.; Mingo, N.; Lofgreen, K.; Volz, S.; Cleri, F.; Keblinski, P. Turning Carbon Nanotubes from Exceptional Heat Conductors into Insulators. *Phys. Rev. Lett.* **2009**, *102*, 105901–4.
- (34) Volkov, A. N.; Zhigilei, L. V. Heat Conduction in Carbon Nanotube Materials: Strong Effect of Intrinsic Thermal Conductivity of Carbon Nanotubes. *Appl. Phys. Lett.* **2012**, *101*, 043113–5.
- (35) Kremer, K.; Grest, G. S. Dynamics of Entangled Linear Polymer Melts: A Molecular Dynamics Simulation. *J. Chem. Phys.* **1990**, *92*, 5057–5086.
- (36) Doi, M.; Edwards, S. F. *The Theory of Polymer Dynamics*; Oxford Science Publications: Oxford, 1986.
- (37) Cahill, D. G.; Watson, S. K.; Pohl, R. O. Lower Limit to the Thermal Conductivity of Disordered Crystals. *Phys. Rev. B: Condens. Matter Mater. Phys.* **1992**, *46*, 6131–6140.
- (38) Braun, J. L.; Rost, C. M.; Lim, M.; Giri, A.; Olson, D. H.; Kotsonis, G. N.; Stan, G.; Brenner, D. W.; Maria, J. P.; Hopkins, P. E. Charge-Induced Disorder Controls the Thermal Conductivity of Entropy-Stabilized Oxides. *Adv. Mater.* **2018**, *30*, 1805004–8.
- (39) Fakhri, N.; Tsybolski, D. A.; Cognet, L.; Weisman, R. B.; Pasquali, M. Diameter-Dependent Bending Dynamics of Single-Walled Carbon Nanotubes in Liquids. *Proc. Natl. Acad. Sci. U. S. A.* **2009**, *106*, 14219–14223.

- (40) Liu, H.; Song, H.-L.; Feng, X.; Yang, J. Surface Effects on the Persistence Length of Nanowires and Nanotubes. *Theor. Appl. Mech. Lett.* **2014**, *4*, 051009–6.
- (41) Ramachandran, R.; Beaucage, G.; Kulkarni, A. S.; McFaddin, D.; Merrick-Mack, J.; Galiatsatos, V. Persistence Length of Short-Chain Branched Polyethylene. *Macromolecules* **2008**, *41*, 9802–9806.
- (42) Brandrup, J.; Immergut, E. H.; Grulke, E. A. *Polymer Handbook*, 4th ed.; Wiley-Interscience: Hoboken, 2003.
- (43) Yang, N.; Li, M.; Patscheider, J.; Youn, S. K.; Park, H. G. A Forest of Sub-1.5-nm-Wide Single-Walled Carbon Nanotubes over an Engineered Alumina Support. *Sci. Rep.* **2017**, *7*, 46725.
- (44) Sugime, H.; Sato, T.; Nakagawa, R.; Hayashi, T.; Inoue, Y.; Noda, S. Ultra-Long Carbon Nanotube Forest *via in Situ* Supplements of Iron and Aluminum Vapor Sources. *Carbon* **2021**, *172*, 772–780.
- (45) Mukherji, D.; Marques, C. M.; Kremer, K. Smart Responsive Polymers: Fundamentals and Design Principles. *Annu. Rev. Condens. Matter Phys.* **2020**, *11*, 271–299.
- (46) Crist, B.; Herena, P. G. Molecular Orbital Studies of Polyethylene Deformation. *J. Polym. Sci., Part B: Polym. Phys.* **1996**, *34*, 449–457.
- (47) Ruscher, C.; Rottler, J.; Boott, C. E.; MacLachlan, M. J.; Mukherji, D. Elasticity and Thermal Transport of Commodity Plastics. *Phys. Rev. Mater.* **2019**, *3*, 125604–7.
- (48) Binder, K. Scaling Concepts for Polymer Brushes and Their Test by Computer Simulation. *Eur. Phys. J. E: Soft Matter Biol. Phys.* **2002**, *9*, 293–298.
- (49) Elliott, I. G.; Kuhl, T. L.; Faller, R. Molecular Simulation Study of the Structure of High Density Polymer Brushes in Good Solvent. *Macromolecules* **2010**, *43*, 9131–9138.
- (50) Manav, M.; Ponga, M.; Phani, A. S. Stress in a Polymer Brush. *J. Mech. Phys. Solids* **2019**, *127*, 125–150.
- (51) Duan, X.; Li, Z.; Liu, J.; Chen, G.; Li, X. Roles of Kink on the Thermal Transport in Single Polyethylene Chains. *J. Appl. Phys.* **2019**, *125*, 164303–6.
- (52) Peierls, R. Zur Kinetischen Theorie der Wärmeleitung in Kristallen. *Ann. Phys.* **1929**, *395*, 1055–1101.
- (53) Allen, P. B.; Feldman, J. L. Thermal Conductivity of Glasses: Theory and Application to Amorphous Si. *Phys. Rev. Lett.* **1989**, *62*, 645–648.
- (54) Simoncelli, M.; Marzari, N.; Mauri, F. Unified Theory of Thermal Transport in Crystals and Disordered Solids. *Nat. Phys.* **2019**, *15*, 809–813.
- (55) Plimpton, S. Fast Parallel Algorithms for Short-Range Molecular Dynamics. *J. Comput. Phys.* **1995**, *117*, 1–19.
- (56) Humphrey, W.; Dalke, A.; Schulten, K. VMD - Visual Molecular Dynamics. *J. Mol. Graphics* **1996**, *14*, 33–38.
- (57) Swope, W. C.; Andersen, H. C.; Berens, P. H.; Wilson, K. R. A Computer Simulation Method for the Calculation of Equilibrium Constants for the Formation of Physical Clusters of Molecules: Application to Small Water Clusters. *J. Chem. Phys.* **1982**, *76*, 637–649.
- (58) Zwanzig, R. Time-correlation Functions and Transport Coefficients in Statistical Mechanics. *Annu. Rev. Phys. Chem.* **1965**, *16*, 67–102.
- (59) Bhardwaj, A.; Phani, A. S.; Nojeh, A.; Mukherji, D. Reduced Thermal Conductivity in Molecular Forests. *arXiv* May 21, **2020**, arXiv:2005.10685.